Electromechanical pendulum for vibration control and energy harvesting

Michele Zilletti[1], Stephen J. Elliott[2], Maryam Ghandchi Tehrani [3]

[1,2,3]*University of Southampton, Institute of Sound and Vibration Research, SO17 1BJ Southampton, UK*

ABSTRACT

This paper presents the design of an experimental electromechanical device for vibration control and energy harvesting. Traditionally, when the broadband resonant response due to a selected mode of a lightly damped structure needs to be controlled a vibration absorber is used. The resonance frequency of the absorber can be chosen to minimise the response of the structure under control. Optimising the damping ratio to achieve this aim also dissipates the most power in the damper, but care must be taken not to exceed the maximum throw of the device at high excitation levels. The absorber may also be mistuned by changes in operation condition and thus underperform. It is thus important to be able to design tuneable vibration absorbers, able to adapt their resonance frequency and their damping ratio depending on the operation condition.

In this paper an electromechanical device consisting of a pendulum connected to an electrical motor is proposed. It is shown that by shunting the terminal of the device with an appropriate electrical circuit it is possible to control both its resonance frequency and its damping ratio. The power dissipated in the resistive part of the shunt circuit could also be harvested and used to implement the tuning mechanism, or for other purposes.

Keywords: *Tuneable vibration absorber, electromechanical absorber, energy harvesting*

1 INTRODUCTION

Dynamic vibration absorbers consists of single degree of freedom systems which are attached to a host structure in order to control its motion [1]. Such devices were originally patented in 1911 [2] and since their invention they have been widely used in different applications such as civil [3-5] and aerospace [6-8] structures just to mention a few. Depending on the application these devices can operate in different ways. For example they can be operated to reduce the motion of the host structure only at a particular forcing frequency, in which case the devices natural frequency is tuned to this excitation frequency and the damping of the device should also be as low as possible. In this case the device is then often known as a ‘‘vibration neutraliser’’. Another way to operate these devices is to attenuate the vibration due to a resonant mode of the structure over a range of frequencies. In this case the devices is sometimes referred to as a ‘‘tuned mass damper’’ (TMD) or ‘‘dynamic vibration absorber’’ (DVA). A vast literature is devoted to the optimal tuning of the natural frequency and damping ratio of these devices. The selected mode of the host structure is generally modelled as a single degree of freedom system for this optimisation, often without any inherent damping. A summary of some of the optimisation criteria can be found in reference [9].

One problem of using these device is that the operating conditions (e.g. temperature, pressure tension in the structure) or changes in excitation frequency may results in a mistuning of their natural frequency and damping which in the worst case may result in an enhancement of the vibration level

[1] Research Scientist, m.zilletti@soton.ac.uk

[2], Professor S.J.Elliott@soton.ac.uk

[3] Lecturer, M.Ghandchi-Tehrani @soton.ac.uk

* Corresponding author

of the host structure. For this reason adaptive tuned vibration absorbers (ATVAs) have been proposed to adaptively tuning their stiffness and damping depending on the system state [5, 7]. Considerable ingenuity has been put into tuning the stiffness and damping of ATVAs [10-12]. Some of the solutions suggest to vary, the shape of the suspension [13], the number of the active coil in the spring [10] or using magneto-rheological fluid [11]. These solutions may add complexity and increase the cost of these devices for a limited tuneable range of their natural frequency and damping ratio.

Electromagnetic devices can also be used as ATVAs by connecting an appropriate shunt circuit to the transducer terminals. Different types of shunt can be used in order to change the resonance frequency and damping ratio of the absorber. The shunt may include passive resistive, capacitive or inductive loads for example. In this case the tunable range may be limited by the electro-mechanical coupling of the transducer used thus, synthetic electrical circuits, which can potentially provide very high capacitance and inductance as well as negative electrical circuit elements may be employed. Some example of these devices can be found in references [12, 14-20].

Another control approaches involving electromagnetic devices is the use of switching shunt electronics where the shunt impedance can be rapidly switched or gradually swept through different values. This technique has been successfully implemented, even though requires fast digital logic, more complicated switching circuitry and introduces nonlinearities into the system [21-26].

Even if the use of synthetic circuits may increase the performance of the ATVAs particular care must be taken in ensuring the stability of the system especially when negative values of the electrical components are used. Also another drawback is that they require external energy to operate.

It has been previously shown that rotational electro-magnetic motor offers a higher electro-mechanical coupling compared to linear motor of equivalent weight [27]. This suggests that passive electrical circuits may be used to shunt rotational motors allowing changes of the resonance frequency and damping ratio of the absorber in a wider rage compare to a linear absorber. In this paper a preliminary study on the design of an adaptive pendulum absorber using a shunted DC motor is presented.

The paper is divided in 6 sections. In section 2 the experimental set-up is described. In section 3 the mathematical model is derived and is validated against measured data in section 4. Section 5 presents simulation results on the use of a capacitive load to change the dynamics of the absorber. Final conclusions are given in section 6.

2 EXPERIMENTAL SETUP

The vibration absorber considered in this paper consists of a pendulum connected to a DC electrical motor. A picture of the experimental set-up is shown in Figure 1(a).

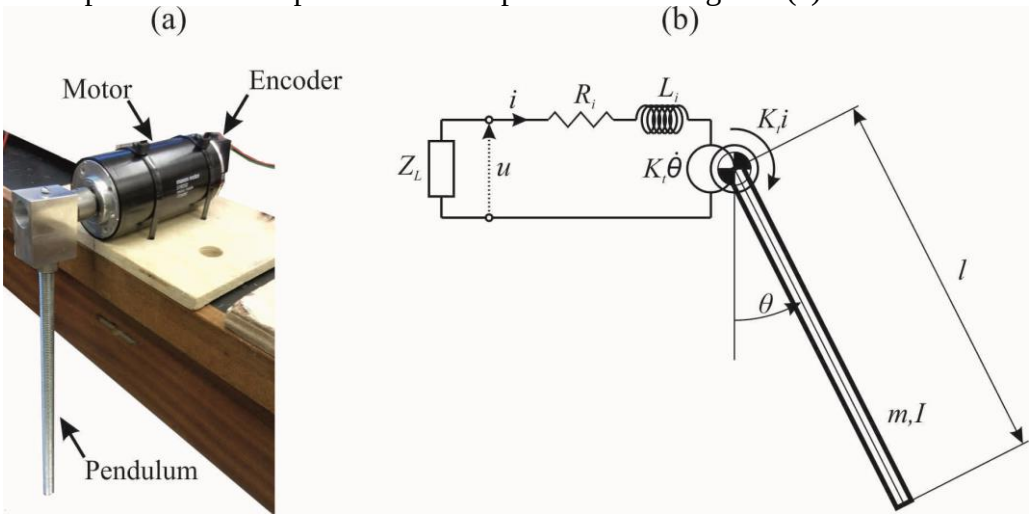

Figure 1 - (a) Experimental pendulum; (b) electromechanical scheme of the pendulum

The motor used for this application is a Maxon DC motor (model 353301) which is equipped with an encoder (model HEDS 5540) to measure the rotation of the pendulum around the pivot. The physical and geometrical parameters of the electro-mechanical pendulum are summarised in Table 1. Figure 1(b) shows a scheme of the pendulum with moment of inertia I and mass m. Also shown is the electrical circuit of the motor including the internal resistance R_i and inductance L_i of the coil and the shunt impedance Z_L connected to the terminals of the motor. The electro-mechanical coupling produces a voltage proportional to the rotational velocity of the pendulum $\dot{\theta}$ and generates a moment on the pendulum proportional to the current i flowing in the electrical circuit via the coupling coefficient K_t. In the next section the equation of motion of the electro-mechanical pendulum are derived.

Table 1 - Physical and geometrical parameters of the electromechanical pendulum

Parameter	**Value**
Pendulum	
Mass	$m = 0.22$ kg
Length	$l = 0.35$ m
Gravitational acceleration	$g = 9.81$ m/s^2
Natural frequency	f_n =1.05 Hz
Moment of inertia	$I = 0.0084$ kg m^2
Viscous damping	$c = 1.92 \times 10^{-4}$ Nms/rad
Fiction damping coefficient	$c_t = 0.018$ Nms/rad
Static friction coefficient	k_s =0.1 Nm
Minimum velocity	$\dot{\theta}_s = 0.5$ rad/s
Motor	
Make	Maxon DC motor
Model	353301
Electrical resistance	$R = 1.8\ \Omega$
Coupling coefficient	$K_t = 245 \times 10^{-3}$ Nm/A
Encoder	
Make	Maxon sensors
Model	HEDS 5540
Counts per turn	500

3 MATHEMATICAL MODEL

In this section the mathematical model of the electromechanical pendulum absorber is derived. With reference to figure 1(b) the equation of motion of the pendulum can be written as:

$$I\ddot{\theta} + f(\dot{\theta}) + k\sin(\theta) = N \tag{1}$$

where θ is the rotation of the pendulum in radiant, I is the moment of inertia given by $I = ml^2/3$ where m and l are the mass and the length of the pendulum respectively and $k = \frac{mgl}{2}$ where g is the gravitational acceleration. Finally $f(\dot{\theta})$ is a nonlinear damping function of the rotational velocity of the pendulum to be identified based on experimental measurements. The moment applied by the electrical motor to the pendulum due to the back electromotive force can be written as:

$$N = K_t i \tag{2}$$

where K_t is the electromechanical coupling of the motor and i is the current flowing in the motor coil. From the scheme in figure 1 (b) the voltage u across the terminals of the motor can be expressed by:

$$u = R_i i + K_t \dot{\theta} \tag{3}$$

where R_i is the internal electrical resistance of the coil. Since the effect of the inductance on the dynamics of the pendulum in the frequency around the natural frequency of the pendulum is negligible, the inductive term in equation (3) has been neglected.

In order to vary the resonance frequency of the pendulum a capacitive shunt can be connected to the terminal of the motor. In this case the voltage across the motor terminals can be written as:

$$u = -\frac{1}{C_L}\int i\, dt \tag{4}$$

where C_L is the capacitance of the shunt. Substituting equation (4) in (3) the current i can be written as:

$$i = -\frac{1}{C_L R_i}\int i\, dt - \frac{K_t}{R_i}\dot{\theta} \tag{5}$$

Substituting equation (5) in (2) and then in (1) yields

$$I\ddot{\theta} + f(\dot{\theta}) + k\sin(\theta) = -\frac{K_t}{C_L R_i}\int i\, dt - \frac{K_t^2}{R_i}\dot{\theta} \tag{6}$$

Rearranging the terms in equation (7), the angular acceleration can be written as:

$$\ddot{\theta} = -\frac{K_t}{I C_L R_i}\int i\, dt - \frac{K_t^2}{I R_i}\dot{\theta} - \frac{f(\dot{\theta})}{I} - \frac{k}{I}\sin(\theta) \tag{7}$$

3.1 Identification of the damping force

In this subsection a model of the damping function $f(\dot{\theta})$ is identified based on experimental measurements. The equation of motion in open circuit condition is given by:

$$I\ddot{\theta} + f(\dot{\theta}) + k\sin(\theta) = 0 \tag{8}$$

and thus the damping function $f(\dot{\theta})$ can be calculated as:

$$f(\dot{\theta}) = -I\ddot{\theta} - k\sin(\theta)\,. \tag{9}$$

Imposing an initial condition of zero velocity and $\pi/2$ radiant displacement, the angular displacement, θ, shown in Figure 2 (a) has been measured using the encoder. Figure 2 (b) shows the angular acceleration obtained by a double time derivative of the angular displacement. Since the encoder gives 500 pules per turns the displacement signal is characterised by a step pattern.

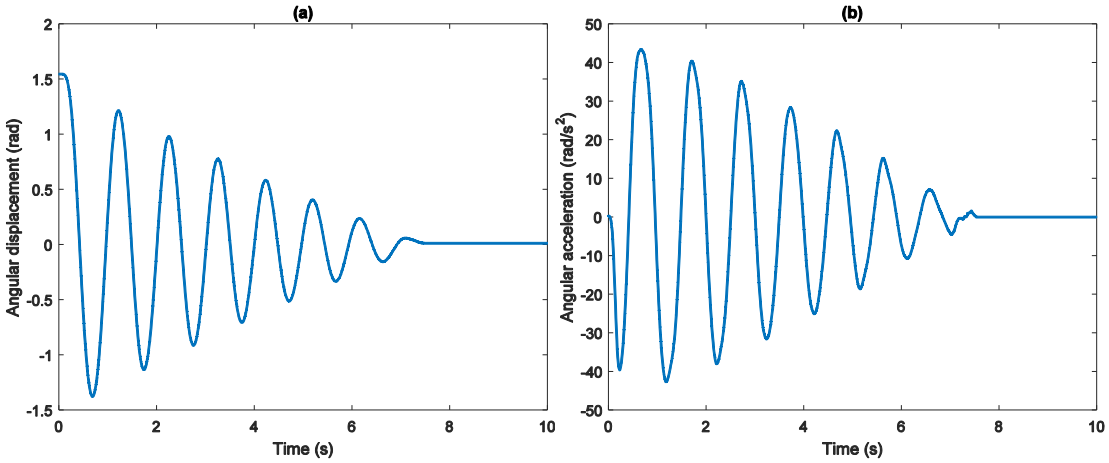

Figure 2 - time history of (a) angular displacement and angular acceleration for an initial displacement of about $\pi/2$ radiant displacement.

Therefore the time derivative of such a signal tends to a infinity value at every pulse of the encoder thus the displacement signal needs to be smoothed before a time derivative is performed. It is important that both the acceleration and the displacement are both smoothen with the same filter

in order to avoid time delays between the two signals which may lead to an incorrect estimate of the damping function in equation (9).

The solid line in figure 3 shows the damping function as a function of the angular velocity. The plot shows that the damping function is characterised by a viscous damping plus a friction type damping. It is therefore assumed that the damping function is given by:

$$f(\dot{\theta}) = c_s\dot{\theta} + c_t \tanh(\dot{\theta}) \tag{10}$$

where the viscous damping coefficient c_s and the friction damping coefficient c_t given in table 1 are obtained by a curve fitting to the measurement. The theoretical model of the damping force is shown by the dashed line in figure 3.

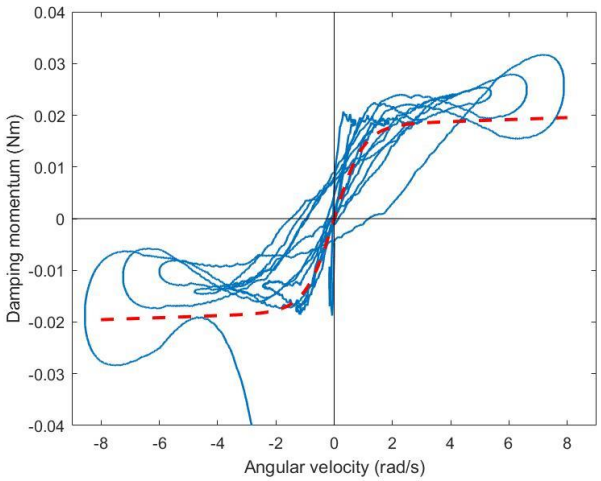

Figure 3 - measured damping force (solid line) and curve fitting (dashed line)

Substituting equation (10) in (7) the angular acceleration can be written as:

$$\ddot{\theta} = -\frac{K_t}{IC_LR_i}\int i\,dt - \frac{K_t^2}{IR_i}\dot{\theta} - \frac{c\dot{\theta} + c_t\tanh(\dot{\theta})}{I} - \frac{k}{I}\sin(\theta) \tag{11}$$

Equation (11) can be rewritten using a state space formulation as:

$$\dot{\boldsymbol{x}} = \boldsymbol{A}\boldsymbol{x} + \boldsymbol{K}\sin(\boldsymbol{x}) + \boldsymbol{C_t}\tanh(\boldsymbol{x}) \tag{12}$$

where the state vector is $\boldsymbol{x} = [\theta \quad \dot{\theta} \quad \int i\,dt]^T$ and the state space matrices are given by:

$$\boldsymbol{A} = \begin{bmatrix} 0 & 1 & 0 \\ 0 & -c/I - \frac{K_t^2}{IR_i} & -\frac{K_t}{IC_LR_i} \\ 0 & -\frac{K_t}{R_i} & -\frac{1}{C_LR_i} \end{bmatrix} \quad \boldsymbol{K} = \begin{bmatrix} 0 & 0 & 0 \\ -\frac{k}{I} & 0 & 0 \\ 0 & 0 & 0 \end{bmatrix} \quad \boldsymbol{C_t} = \begin{bmatrix} 0 & 0 & 0 \\ 0 & -c_t/I & 0 \\ 0 & 0 & 0 \end{bmatrix} \tag{13}$$

In order to take into account the static friction of the pendulum the following condition in the numerical simulations has be used:

$$\text{if } |\dot{\theta}| < \dot{\theta}_s \text{ and } |k\sin(\theta)| < k_s \;\Rightarrow\; \theta(n+1) = \theta(n) \text{ and } \dot{\theta}(n+1) = 0 \tag{14}$$

where n is the number of iteration $\dot{\theta}_s$ is the velocity before the pendulum stops and k_s is the static force obtained from experimental data.

4 MODEL VALIDATION

In this section the model identified in the previous section is validated against experimental measurements. In this early stage of the design of the electro-mechanical absorber it was not been possible to excited the pendulum imposing a displacement of the pivot therefore the tests were

conducted imposing an initial angular displacement. The dashed line in Figure 4 shows the time history of the measured (a) displacement, (b) velocity, (c) acceleration and (d) voltage when an initial displacement of about $\pi/2$ radiant is imposed. The solid line shows the same quantities obtained from the numerical integration of the equation of motion of the system with the same initial conditions. The graphs show that the experimental a simulated results are in a reasonable agreement.

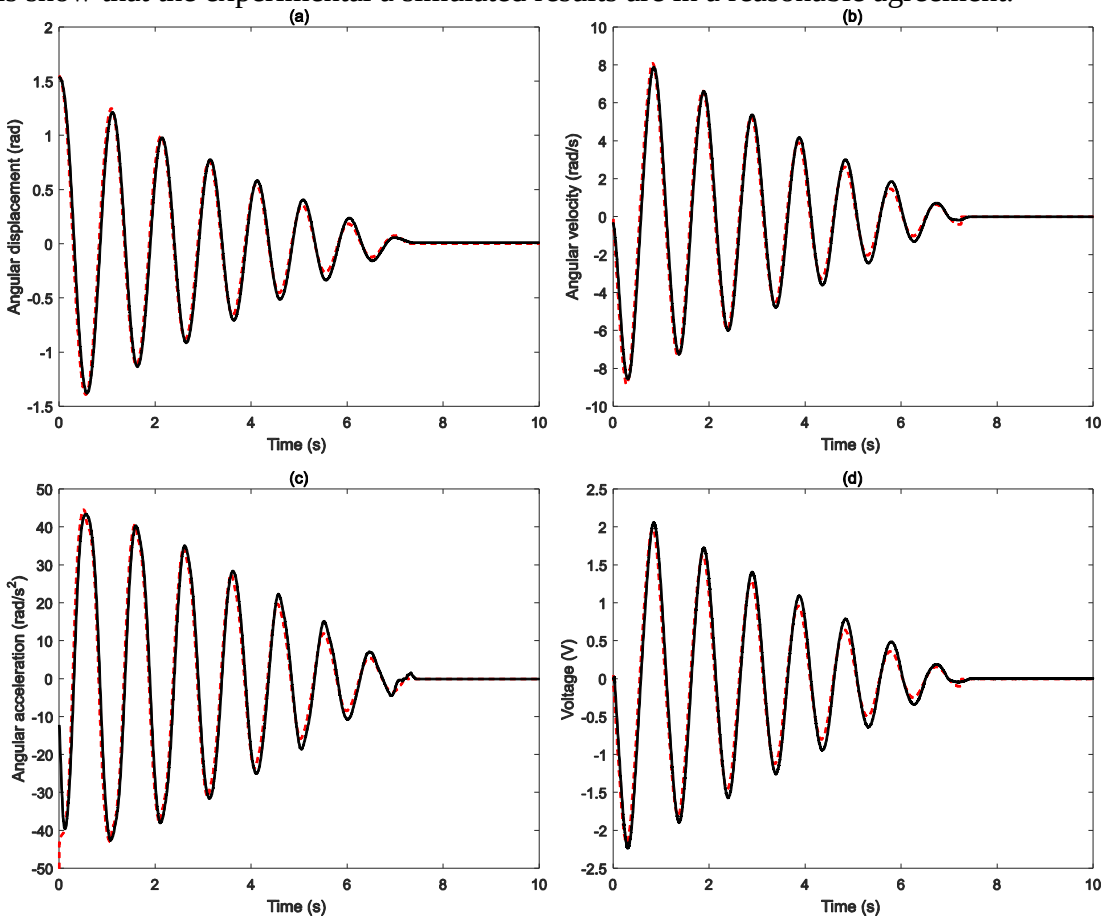

Figure 4 - measured (dashed line) simulated (solid line) (a) displacement, (b) velocity, (c) acceleration and (d) voltage for an initial condition of about $\pi/2$ displacement in open circuit condition.

Figure 5 shows the measured (dashed line) and simulated (solid line) time history of the (a) displacement, (b) velocity and (c) acceleration when the terminal of the electrical motor are short circuited. Once again the measured and simulated results are in agreement. The plots shows a small discrepancy between the model and experimental data in predicting the static behavior of the pendulum once the oscillation has fed away. Comparing the behavior of the pendulum from the open circuit condition, shown in figure 4, to the short circuit condition, shown in figure 5, it can be noticed that the effect of the shunt is to damp the oscillation of the pendulum due to the electromechanical coupling of the DC motor. This suggest that by varying the value of the shunt resistance it is possible to accurately tune the mechanical damping of the absorber. In the next section the effect of a shunt capacitor is taken into account in order to vary the resonance frequency of the absorber.

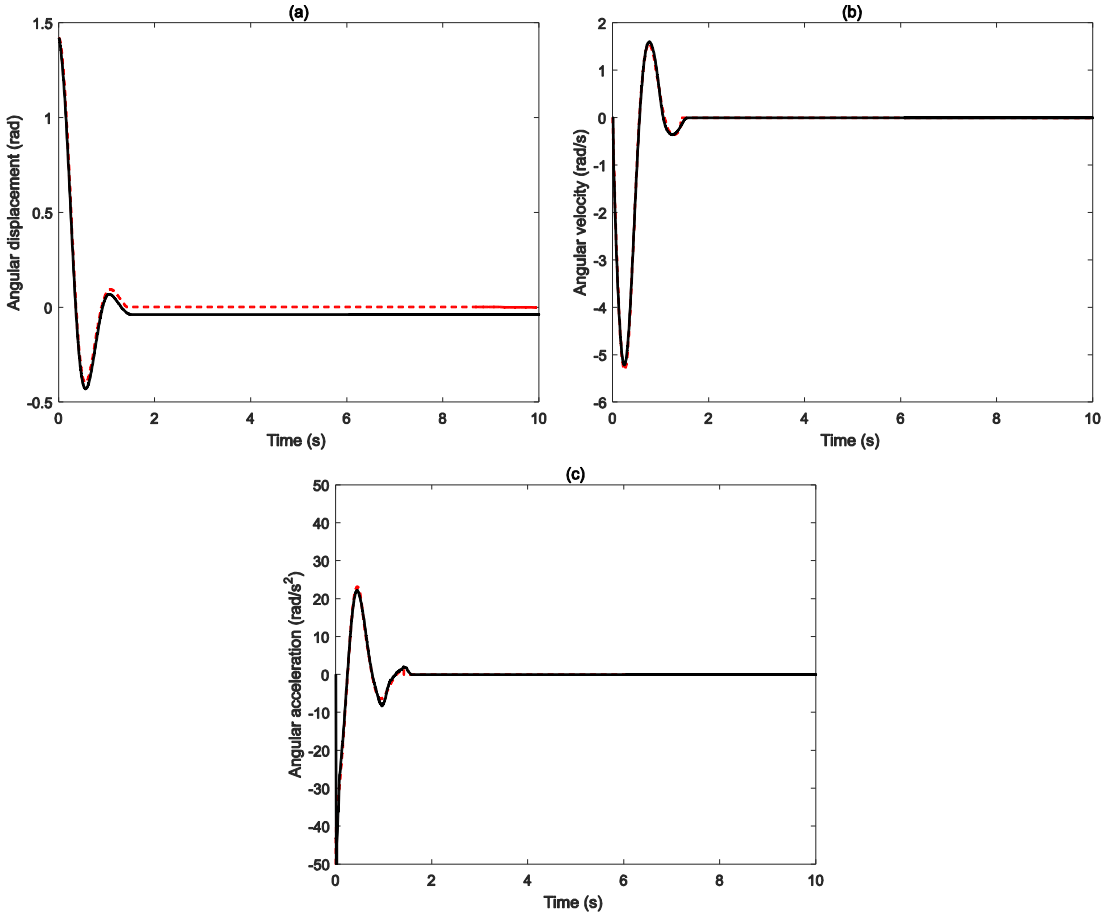

Figure 5 - measured (dashed line) simulated (solid line) (a) displacement, (b) velocity, (c) acceleration and (d) voltage for an initial condition of about $\pi/2$ displacement in short circuit condition.

5 NUMERIACAL SIMULATION OF A CAPACITIVE SHUNT

In this section the effect of a capacitor shunt on the dynamics of the absorber is considered. In this early stage of the absorber design only simulation results are shown in this section.

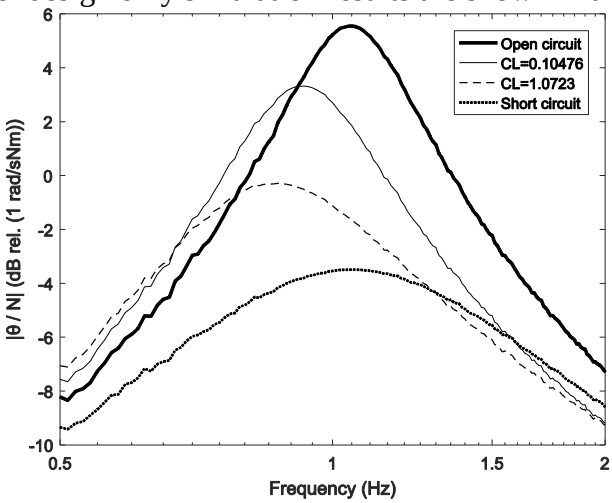

Figure 6 - frequency response function between the angular velocity and a harmonic excitation moment at different frequencies and amplitude of 0.02 Nm. Open circuit (solid line), shunted with a capacitance of 0.1 F (faint line), 1 F (dashed line), short circuit (dotted line)

Figure 6 shows the simulated frequency response function (FRF) between the angular velocity of the pendulum and an excitation moment applied at the pendulum pivot for different values of the shunt capacitor. The tick line in figure 6 shows that when the terminals of the motor are disconnected (open circuit) the response of the absorber is characterized by a single lightly damped resonance peak. When a capacitive shunt is connected to the terminals of the motor and is progressively increased the resonance frequency of the absorber is shifted down in frequency. Together with the change of the pendulum resonance frequency, the effect of the capacitive shunt is also to damp the response of the system. If the shunt capacitance is further increased the effect of the shunt is to increase the damping in such a way that almost no shift in the resonance frequency is visible anymore. If the value of the shunt capacitance tends to infinity, thus the impedance of the shunt tends to zero, the motor is short circuited and the damping in the system is maximised.

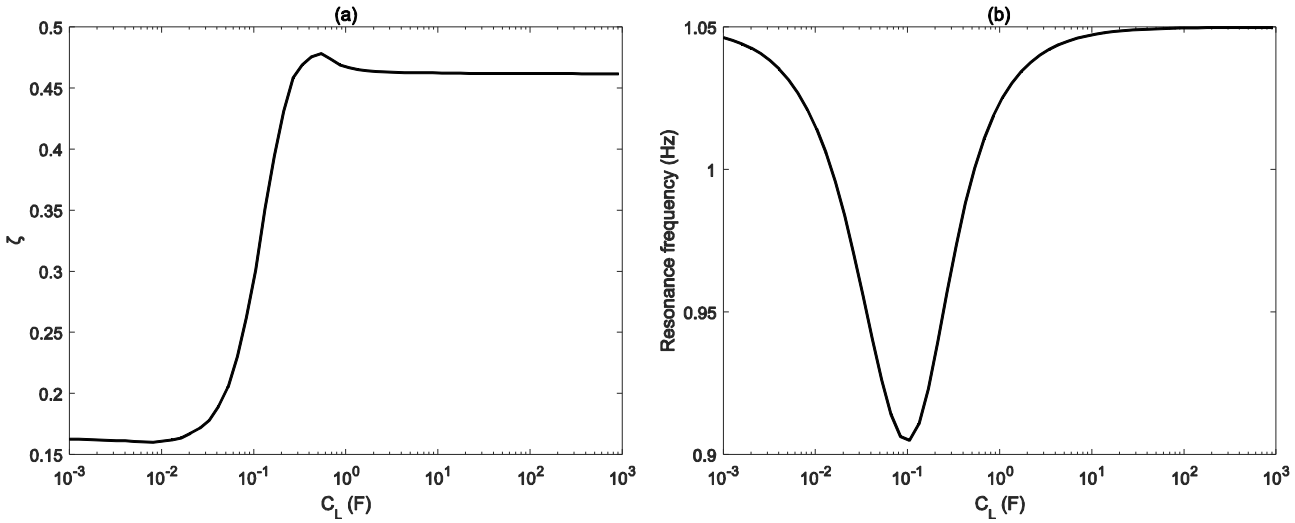

Figure 7: (a) damping ratio and (b) resonance frequency as a function of the capacitive load

Figure 7 shows (a) the damping ratio and (b) the resonance frequency of the absorber as a function of the capacitive shunt. The graphs shows that the damping ratio increases from about 16 % in the open circuit condition to about 45% when the motor terminals are short circuited. As the shunt capacitor is increased the resonance frequency of the absorber starts to decreases until it reaches a minimum when $C_L = 0.1$ F and increases again as the shunt capacitor is further increased.

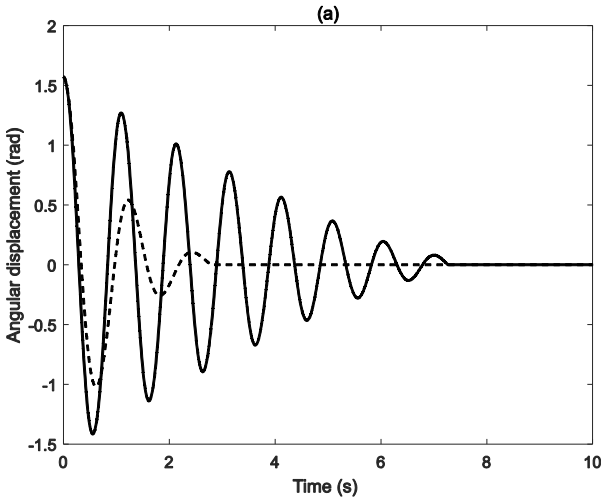

Figure 8 - Angular displacement open circuit (solid line) and with a 0.1 F capacitor (dashed line) for an initial condition of $\pi/2$ radiant displacement and zero velocity

Figure 8 shows the time history of the angular displacement in open circuit (solid line) and when a shunt capacitor of 0.1 F is connected to terminals (dashed line) when an initial angular displacement of $\pi/2$ radiant is imposed. The graph confirms that the effect of the capacitor is to reduce the resonance frequency as well as to damp the response of the absorber.

6 CONCLUSION

This paper has presented an initial study on the design of a tuneable pendulum vibration absorber. The absorber consists of a pendulum connected to a DC motor. The equation of motion of the system has been derived and a damping model has been identified from the experimental data. It has been experimentally shown that by connecting a resistive load it is possible to vary the damping of the absorber from about 16% in open circuit condition to 45% in short circuit condition.

Simulation results has shown that by connecting a pure capacitive load to the terminals of the motor it is possible to reduce the resonance frequency of the absorber by about 10%. Together with a decrease of the resonance frequency an increase of the damping of the device has been also observed.

The experimental implementation of a capacitive load is currently under investigation. Due to the high values of the capacitance, super capacitors may be considered for this application.

ACKNOWLEDGEMENT

The work done by Michele Zilletti was supported by the EPSRC through 'Engineering Nonlinearity' programme grant (EP/K003836/1).

REFERENCES

[1] Den Hartog, J.P., *Mechanical Vibrations*. 4th ed. 1956, New York: McGraw-Hill.

[2] Frahm, H., *Device for damping vibrations of bodies*, U. Patent, Editor. 1911.

[3] Dallard, P., et al., *The London Millennium Footbridge.* Structural Engineer, 2001. **79**(22): p. 17-33.

[4] Spencer, B.F., Jr. and M.K. Sain, *Controlling buildings: a new frontier in feedback.* Control Systems, IEEE, 1997. **17**(6): p. 19-35.

[5] Sun, J.Q., M.R. Jolly, and M.A. Norris, *Passive, Adaptive and Active Tuned Vibration Absorbers---A Survey*. Journal of Vibration and Acoustics, 1995. **117**(B): p. 234-242.

[6] Fuller, C.R., et al., *Control of aircraft interior noise using globally detuned vibration absorber.* Journal of Sound and Vibration, 1997. **203**(5): p. 745-761.

[7] von Flotow, A.H., Beard, A., and Bailey, D. *Adaptive tuned vibration absorbers: tuning laws, tracking agility, sizing and physical implementations*. in *Noise-Con 94*. 1994. Fort Lauderdale, FL.

[8] von Flotow, A.H., et al., *Adaptively tuned vibration absorber for reduction of aircraft cabin noise*. 1999: US Patent 5,873,559.

[9] Zilletti, M., S.J. Elliott, and E. Rustighi, *Optimisation of dynamic vibration absorbers to minimise kinetic energy and maximise internal power dissipation.* Journal of Sound and Vibration, 2012. **331**(18): p. 4093-4100.

[10] Franchek, M.A., M.W. Ryan, and R.J. Bernhard, *ADAPTIVE PASSIVE VIBRATION CONTROL.* Journal of Sound and Vibration, 1996. **189**(5): p. 565-585.

[11] Hirunyapruk, C., et al., *A tunable magneto-rheological fluid-filled beam-like vibration absorber.* Smart Materials and Structures, 2010. **19**(5): p. 055020.

[12] Bo, Y., Z. Xinong, and N. Hongpan, *Design and test of a novel isolator with negative resistance electromagnetic shunt damping.* Smart Materials and Structures, 2012. **21**(3): p. 035003.

[13] Bonello, P., et al., *Designs for an adaptive tuned vibration absorber with variable shape stiffness element.* Proceedings of the Royal Society A: Mathematical, Physical and Engineering Science, 2005. **461**(2064): p. 3955-3976.

[14] Hongpan, N., et al., *A new electromagnetic shunt damping treatment and vibration control of beam structures.* Smart Materials and Structures, 2009. **18**(4): p. 045009.

[15] Zhang, X., H. Niu, and B. Yan, *A novel multimode negative inductance negative resistance shunted electromagnetic damping and its application on a cantilever plate.* Journal of Sound and Vibration, 2012. **331**(10): p. 2257-2271.

[16] Tai-Hong, C. and O. Il-Kwon, *A current-flowing electromagnetic shunt damper for multi-mode vibration control of cantilever beams.* Smart Materials and Structures, 2009. **18**(9): p. 095036.

[17] Cheng, T.H. and I.K. Oh, *Vibration Suppression of Flexible Beam Using Electromagnetic Shunt Damper.* IEEE Transactions on Magnetics, 2009. **45**(6): p. 2758-2761.

[18] Inoue, T., Y. Ishida, and M. Sumi, *Vibration Suppression Using Electromagnetic Resonant Shunt Damper.* Journal of Vibration and Acoustics, 2008. **130**(4): p. 041003-041003.

[19] Elliott, S.J. and M. Zilletti, *Scaling of electromagnetic transducers for shunt damping and energy harvesting.* Journal of Sound and Vibration, 2014. **333**(8): p. 2185-2195.

[20] McDaid, A.J. and B.R. Mace, *A self-tuning electromagnetic vibration absorber with adaptive shunt electronics.* Smart Materials and Structures, 2013. **22**(10): p. 105013.

[21] Zilletti, M. and P. Gardonio, *Experimental implementation of switching and sweeping tuneable vibration absorbers for broadband vibration control.* Journal of Sound and Vibration, 2015. **334**: p. 164-177.

[22] Gardonio, P. and M. Zilletti, *Sweeping tuneable vibration absorbers for low-mid frequencies vibration control.* Journal of Sound and Vibration, 2015. **354**: p. 1-12.

[23] Gardonio, P. and M. Zilletti, *Integrated tuned vibration absorbers: A theoretical study.* The Journal of the Acoustical Society of America, 2013. **134**(5): p. 3631-3644.

[24] Hongli, J., et al., *Multi-modal vibration control using a synchronized switch based on a displacement switching threshold.* Smart Materials and Structures, 2009. **18**(3): p. 035016.

[25] Cunefare, K.A., et al., *State-Switched Absorber for Semi-Active Structural Control.* Journal of Intelligent Material Systems and Structures, 2000. **11**(4): p. 300-310.

[26] Holdhusen, M.H. and K.A. Cunefare, *A State-Switched Absorber Used for Vibration Control of Continuous Systems.* Journal of Vibration and Acoustics, 2007. **129**(5): p. 577-589.

[27] Hendijanizadeh, M., et al., *Output power and efficiency of electromagnetic energy harvesting systems with constrained range of motion.* Smart Materials and Structures, 2013. **22**(12): p. 125009.